Thermodynamic modelling and analysis of a solar organic Rankine cycle employing thermofluids

H. U. Helvaci*, Z. A. Khan

Bournemouth University, Nano Corr, Energy and Modelling, Faculty of Science and Technology, Bournemouth, Bournemouth, BH12 5BB, UK

* Corresponding author: Huseyin Utku Helvaci

Faculty of Science and Technology, Fern Barrow, Talbot Campus, Bournemouth University, Poole, Dorset BH12 5BB

Tel: +44 7473 770009

E-mail address: hhelvaci@bournemouth.ac.uk

ABSTRACT

This paper presents thermodynamic modelling and simulation study of a small scale saturated solar organic Rankine cycle (ORC) which consists of a stationary, flat plate solar energy collector that is utilised as a vapour generator, a vane expander, a water-cooled condenser and a pump. Simulations are conducted under constant condensing temperature/pressure and various cycle pressure ratios (PR) for 24 organic thermofluids including Hydrocarbons (HCs), Hydrofluorocarbons (HFCs), Perfluorocarbons (PFCs), Hydrofluoroethers (HFEs) and Hydrofluoroolefins (HFOs). Special attention is given to the influence of PR and fluids' physical properties on the solar ORC performance as well as fluids' environmental and safety impacts including global warming potential (GWP), flammability and toxicity. The simulation results indicate that when the same fluid is considered, pressure ratio of the cycle leads to various operating conditions such as collector (evaporating) pressure which results in various collector, expander and cycle efficiency. For instance, increasing the pressure ratio of the cycle enhances the net work output and the thermal efficiency of the cycle, whereas it decreases the flat plate collector efficiency. The results also indicate that the proposed system produces the maximum net work output of 210.45W with a thermal efficiency of 9.64% by using 1-butene. Furthermore, trans-2-butene, cis-2-butene, R600, R600a, R601, R601a and neopentane (HC), R227ea and R236fa (HFC), RC318 (PFC) and R1234ze (HFO) show promising solar ORC thermal performances. However, the flammability problem of HCs and global warming potential issue of HFCs and PFCs limit their applications, owing to the safety and environmental concerns.

On the other hand, in terms of the environmental impact, thermofluids such as RE347mcc, RE245fa2 (HFEs) and R1234ze, R1233zd (HFOs) offer an attractive alternative, yet they were neither the most efficient, nor generated the highest amount of net work output. This

paper provides thermofluids' selection guidelines to achieve maximum efficiency within solar thermal energy technologies while keeping environmental impacts into considerations.

Keywords: Solar thermal energy; saturated organic Rankine cycle; vane expander; thermofluids

Nomenclature		**Subscripts**	
		a	ambient
A	area, m^2	*col*	collector
Bo	boiling number	*cond*	condensation
C	constant	*crit*	critical
C_b	bond conductance	*cw*	cooling water
C_p	specific heat, J/kg K	*cyc*	cycle
Co	convection number	*dsg*	designed
d	radius of the stator to the centre of the rotor	*evap*	evaporation
D	diameter, m	*exh*	exhaust
e	eccentricity, m	*exp*	expander
f	friction factor	*f*	fluid
F	fin efficiency	*g*	vapour
F'	collector efficiency factor	*i*	inner
F_R	heat removal factor	*in*	inlet, incoming
Fr	Froude number	*int*	intake
G	mass flux, kg/m^2 s	*is*	isentropic
h_{sp}	single phase heat transfer coefficient, W/m^2K	*l*	liquid
h_{tp}	two phase heat transfer coefficient, W/m^2K	*lat*	latent
$h_{nc,B}$	nucleate boiling factor	*max*	maximum
$h_{c,B}$	convective boiling factor	*mec*	mechanical
h	enthalpy, J/kg	*nbp*	Normal boiling point
h_{fg}	heat of vaporisation, J/kg	*o*	outer
k	thermal conductivity, W/m K	*out*	outlet
k_{ratio}	heat capacity ratio	*ov*	over
$\dot{m}$	mass flow rate, kg/s	*p*	plate
M	molecular weight, g/mol	*pp*	pinch point
N	dimensionless parameter	*rot*	rotor
n	number of vanes	*s*	isentropic
Nu	Nusselt number	*snb*	sensible
ORC	organic Rankine cycle	*sp*	single phase
P	Pressure, bar	*stat*	stator
PR	pressure ratio	*t*	top
Pr	Prandtl number	*tp*	two phase
r	radius, m	*T*	total
$r_{v,built\text{-}in}$	built-in ratio of the expander	*u*	useful
Re	Reynolds number	*ud*	under
S	solar radiation, W/m^2	*wf*	working fluid

T	temperature, ºC		
U	heat loss coefficient, W/m^{2}K	**Greek symbols**	
$\dot{Q}$	heat, W	υ	kinematic viscosity, m^2/s
v	velocity, m/s	ν	specific volume, m^3/kg
V	volume, m^3	ϕ	heat flux, W/m^2
W	tube spacing	ρ	density, kg/m^3
$\dot{W}$	work, kW	γ	angle between the vanes, deg
x	vapour quality	θ	angle of a specific vane from the origin

1. Introduction

The World has been facing numerous environmental problems such as air pollution, ozone layer depletion, acid rain and global warming, mainly due to increasing consumption of fossil fuels [1]. Extracting fossil fuels in the future will become gradually challenging. Increasing demands of energy from non-renewable sources remain unsustainable. Therefore utilising renewable energy sources as an alternative has been of great importance for domestic heating and electricity generation [2, 3].

Renewable energy sources such as solar thermal, geothermal, biomass and waste heat can be categorised as low-grade temperature energy sources and they have potential in reducing consumption of fossil fuels [4, 5]. However, conventional Rankine cycle is not an economical and efficient alternative for the conversion of heat from renewable energy sources [4]. A conventional Rankine cycle employing organic compounds rather than water is called as organic Rankine cycle (ORC) and it is the most accepted technology for converting low-grade heat energy source into mechanical work [6].

A considerable amount of research has been conducted on the installation of solar ORCs where non-stationary flat plate collectors are used as a heat source of the cycle. Experimental study on the performance of such systems with a selected pure fluid including various types of organic compounds such as HFCs (R134a, R245fa), HFEs (HFE 7000) and inorganic compounds (CO_2) has been conducted. Manolakos et al. conducted an experimental study on

a low-grade solar ORC using pure R-134a as the working fluid. The generated mechanical work is utilised for reverse osmosis (RO) desalination [7-9]. Wang et al. designed and constructed a solar sourced ORC, where R245fa is used as the working fluid of the system. They reported that 1.64 kW average shaft output was obtained from the new designed R245fa expander [10]. Another experimental study of a small scale solar ORC using R245fa is established by [11]. The effect of a recuperator for the constant flow rate condition was analysed in their study, it was concluded that the recuperator does not lead to an increase in the thermal efficiency of the system [11]. Yamaguchi et al. conducted an experimental study on supercritical solar ORCs, using CO_2 [12]. Another solar ORC, utilising inorganic fluid (CO_2) was also investigated in Ref. [13]. In both studies it is concluded that CO_2 offers a feasible alternative to be used in solar thermal power applications.

On the other hand, selection of the most suitable working fluid for solar ORCs and optimisation of the system for various operating conditions, including both simulation and experimental studies has attracted many researchers. Rayegan [14] compared 117 organic fluids on the basis of their effects on thermal efficiency, net power output and exergetic efficiency of the solar ORC. They claimed that fluids with higher critical temperature were considered to be the best [14]. Torres [15] presented a theoretical study of solar ORC where solar collector is used as thermal energy source of the cycle. In their analysis, they considered four different models of stationary solar collectors with twelve substances, including organic (HCs and HFCs) and inorganic (ammonia) fluids. Aperture area needed per unit of mechanical power output was set as a comparison criteria and it was generalised that dry fluids need lower values of the unit aperture area than wet fluids. Marion et al. carried out both theoretical and experimental analyses to show the potential of generating mechanical energy by combining a solar thermal flat plate collector with an organic Rankine cycle. The cycle was simulated by using three organic fluids which were R134a, R227ea and R365mfc.

In order to investigate the optimum operating conditions, a parametric optimisation was conducted. It was found that R365mfc gives the highest performance and it is followed by R134a and R227ea. They also reported that net mechanical power work generation highly depends on the working fluid flow rate [16]. A mathematical model was presented to simulate a solar-sourced regenerative ORC by [17]. In their study they performed a parametric analysis of the system by using different working fluids. They also presented an optimisation study where the daily average efficiency was set as the objective function. It was reported that R245fa and R123 was recommended as the most suitable fluids for the proposed system. They also claimed that turbine inlet pressure and condensation temperature have an effect on the system performance [17]. Another working fluid selection study was conducted by [18]. They modelled the solar organic Rankine cycle with fifteen organic fluids and evaluated the thermodynamic performance of the system for each case. It was reported that R134a and R245fa are the most suitable working fluids [18]. In another study of working fluid selection for solar ORC, R134a was found to be the most appropriate working fluid [19]. It is also concluded that although hydrocarbons such as R600, R600a and R290 show good performance characteristics they need safety measures due to their high flammable nature.

Previously, a theoretical and simulation study of multiphase flow (single and two-phase) in a flat plate collector was conducted and the effect of single and two-phase flows on the heat transfer coefficients, as well as the collector performance was investigated for two working fluids (R134a and HFE 7000) [20]. In the current study, the previous work is extended by modelling a small scale solar ORC, where the flat plate collector is connected directly to the cycle. The simulation analysis of the cycle, using 24 working fluids is conducted under various pressure ratio points. Special attention is given to the effect of the system pressure ratio on the collector efficiency, expander efficiency, net work output of the

cycle and the cycle efficiency. Investigation of the most suitable working fluid for a small scale solar ORC is also discussed in terms of its thermo-physical and environmental properties. This research is also expected to demonstrate the potential of solar ORCs where flat-plate collectors can be either mounted on or integrated into a roof of a commercial or residential building to generate mechanical and heat energy simultaneously by utilising environmentally friendly thermo-fluids.

2. Mathematical modelling

2.1. Solar organic Rankine cycle

The proposed small scale saturated solar ORC is made up of four components which are a solar collector, a pump, a condenser and an expander (Figure 1).

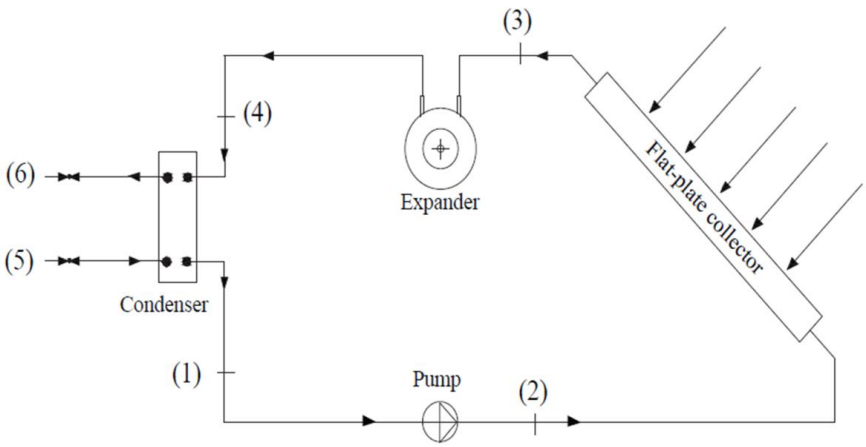

Figure 1 A schematic diagram of the proposed solar ORC

In the proposed system, the solar collector is utilised as an evaporator of the cycle where pressurised vapour is directly generated. This configuration is called 'Direct vapour generation' (DVG) and has been studied and recommended by various researchers [15, 16] due to its advantage of eliminating additional heat exchanger (evaporator) which would cause extra cost and heat losses. As represented in Figure 1, the liquid working fluid is pressurised by the pump and is then sent to the flat plate collector (1—›2). In the collector, solar radiations are converted to thermal energy and this energy is then transferred to the working fluid. The working fluid is preheated and evaporated within the collector tube (2—›3). Then,

the pressurised saturated vapour reaches the expander and turns the expander shaft to generate mechanical energy. This mechanical work could be used to produce electricity when the expander shaft is connected to a generator (3—›4). In the condenser, low pressure exhaust vapour coming from the expander is condensed to saturated liquid with a constant pressure (4—›1). The working fluid is cooled by cold water as it circulates through the condenser (5—›6). Finally, the working fluid is pumped back to the collector to start a new cycle (1—›2). The thermodynamic process of the saturated organic Rankine cycle on T-s diagram is represented in Figure 2.

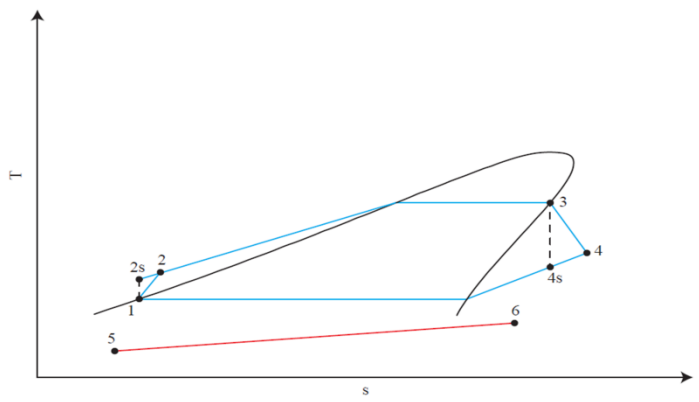

Figure 2 A typical T-s diagram of saturated ORC (for HFE 7000)

Each component of the system is modelled by considering the following assumptions:

- The system is considered as a steady state
- Pressure drops in the collector, condenser and the pipelines have been neglected

2.2. Flat plate collector

The serpentine flat plate collector is previously modelled and represented comprehensively in [20]. The collector consists of a glass cover, absorber plate, copper tube and insulation as it is shown in Figure 3.

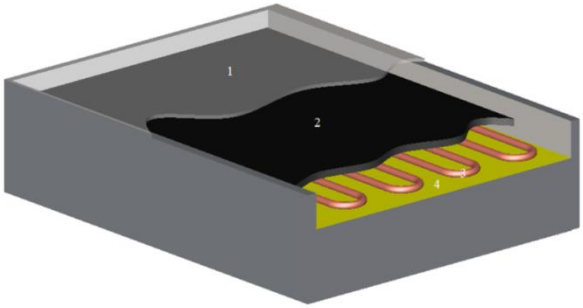

Figure 3 Schematic of the serpentine tube flat plate collector [20]

As the incoming solar radiation travels through the glass cover (1) some portion of this heat is lost to the atmosphere and the remaining is absorbed on the absorber plate (2). Solar energy on the absorber plate surface is calculated as;

$$\dot{Q}_p = A_p\left[S_{in}(\tau\alpha) - U_T\left(T_p - T_a\right)\right] \quad (1)$$

where A_p is the collector plate area, S_{in} is the incoming solar radiation on the collector and $(\tau\alpha)$ is the transmittance-absorbance product. U_T represents the total heat loss coefficient, T_p and T_a represent the plate and ambient temperature respectively. Since the heat loss through the edges has been neglected in this study, the total heat loss coefficient is found to be below:

$$U_T = U_{top} + U_{back} \quad (2)$$

U_{top} and U_{back} can be calculated by the formula developed by Klein [21].

Absorbed solar energy on the collector plate (2) is transferred to the working fluid as it circulates along the collector tube (3). This is called “useful energy gain” of the fluid and it is estimated as;

$$\dot{Q}_u = A_p F_R\left[S_{in}(\tau\alpha) - U_T\left(T_{f,in} - T_a\right)\right] \quad (3)$$

where F_R represents the collector heat removal factor and $T_{f,in}$ represents the working fluid collector inlet temperature.

Collector heat removal factor is found to be as below:

$$F_R = \frac{\dot{m}C_p}{A_p U_T}\left[1 - exp\left(-\frac{A_p U_T F'}{\dot{m}C_p}\right)\right] \quad (4)$$

In Eq. (4), F' is the collector efficiency factor and it can be calculated as:

$$F' = \frac{(U_T)^{-1}}{W[U_T(D_0+(W-D_0)F)]^{-1}+(C_b)^{-1}+(\pi D_i h_f)^{-1}} \quad (5)$$

where W is tube spacing, D_o and D_i is the outer and inner tube diameter respectively. C_b represents the bond conductance and it is neglected ($1/C_b=0$) in the calculation.

F is the fin efficiency and it is determined by Eq. (6):

$$F = \frac{tanh[m(W-D_0/2)]}{m(W-D_0/2)}, \qquad \text{where } m = \sqrt{\frac{U_T}{k\delta}} \quad (6)$$

In Eq. (5), h_f represents the convective heat transfer coefficient of the fluid in the collector tube. As mentioned previously, the flat plate collector is utilised as an evaporator of the solar thermal cycle where the phase change of the fluid takes place. Therefore, the convective heat transfer coefficient (h_f) is evaluated for both single and two phase flows separately in the model.

2.2.1. Single-phase flow

The heat transfer coefficient in the single phase region for fully developed laminar flow and for fully developed turbulent flow are calculated respectively as follows [22]:

$$Nu = 4.36 \qquad \text{where } Re<2300 \quad (7)$$

$$Nu = \frac{\left(\frac{f}{8}\right)(Re-1000)Pr}{1+12.7\left(\frac{f}{8}\right)^{0.5}\left(Pr^{2/3}-1\right)} \qquad \text{where } (3\times10^3<Re<5\times10^6),\ (0.5<Pr<2000) \quad (8)$$

In the calculations the Reynolds number is estimated as:

$$Re = \frac{VD}{\upsilon} \quad (9)$$

and the Prandtl number is defined as:

$$Pr = \frac{\rho \upsilon C_p}{k} \quad (10)$$

where v is the flow velocity, υ is the kinematic viscosity, ρ is the density, C_p is the specific heat of the working fluid and k is the thermal conductivity.

The single phase heat transfer coefficient of the working fluid in the collector tube is calculated with the following equation:

$$h_{sp} = Nu\frac{k}{D} \tag{11}$$

2.2.2. *Two-phase flow*

Calculation of two-phase flow heat transfer coefficient (h_{tp}) is based on the model represented by Shah [23]. The model consists of two distinct boiling mechanisms (nucleate and convective) relies on the calculation of a range of dimensionless parameters.

The dimensionless parameter (N) is calculated according to the conditions of Froude number Fr_l.

$$Fr_l = Froude\ number = \frac{G^2}{\rho^2 g D} \tag{12}$$

where;

$Fr_l < 0.04$ $\quad N = 0.38(Fr_l)^{-0.3}Co$ (13)

$Fr_l > 0.04$ $\quad N = Co$ (14)

Convection number is calculated as follows;

$$Co = \text{Convection number} = \left(\frac{1}{x} - 1\right)^{0.8}\left(\frac{\rho_g}{\rho_l}\right)^{0.5} \tag{15}$$

Then, nucleate boiling ($h_{nc,B}$) and convective boiling ($h_{c,B}$) factors are determined at the following cases;

<u>*Case 1*</u> (N > 1)

$h_{nc,B} = (230Bo^{0.5}) \times h_l$ where Bo > 0.0003 (16a)

$h_{nc,B} = (1 + 46Bo^{0.5}) \times h_l$ where Bo < 0.0003 (16b)

$h_{c,B} = (1..8N^{0.8}) \times h_l$ (16c)

Case 2 (1>N >0.1)

$$h_{nc,B} = (CBo^{0.5}) \times \exp(0.47N^{-0.1}) \times h_l \quad (17a)$$

$$h_{c,B} = (1..8N^{0.8}) \times h_l \quad (17b)$$

Case 3 (N < 0.1)

$$h_{nc,B} = (CBo^{0.5}) \times \exp(2.47N^{-0.15}) \times h_l \quad (18a)$$

$$h_{c,B} = (1..8N^{0.8}) \times h_l \quad (18b)$$

In all three cases, h_l represents the liquid phase heat transfer coefficient and it is calculated by using Dittus-Boelter equation.

The constant C is calculated by using the following equations:

Bo > 0.0011 C = 14.7 (19a)

Bo < 0.0011 C = 15.43 (19b)

where

$$Bo = Boiling\ number = \frac{\phi}{Gh_{fg}} \quad (20)$$

Finally, for each case the nucleate boiling and convective boiling factors are calculated and the larger value is selected. In other words, the larger represents the boiling mechanism and is taken as two-phase flow heat transfer coefficient.

2.3. Expander

The expander is mathematically modelled in the current study, was tested experimentally in a small scale solar organic Rankine cycle using HFE 7000 refrigerant in [24]. The mathematical modelling is divided into two parts which are geometrical and thermodynamic analyses respectively. The former is developed in order to determine the design characteristics and the built-in volume ratio of the expander, whereas the latter is built up to evaluate the expander expansion losses (under or over expansion) where the effect of the operating conditions of the system is taken into account.

The multi-vane expander mainly consists of a stator (cylinder), a rotor and four vanes Figure 4. The rotor is mounted eccentrically in the stator, has radial slots where the vanes are positioned. As the working fluid enters the expander through the inlet port, the rotor as well as the vanes move and compose a working chamber. Due to the continuous rotational movement of the rotor, the area of the working chamber increases until the working fluid begins flowing toward the outlet port. Since then, the area of the working chamber starts to decrease and eventually the vanes close the working chamber. When the fluid begins filling the chamber again after the minimum area of the working chamber is reached, the cycle of the expander is completed [25].

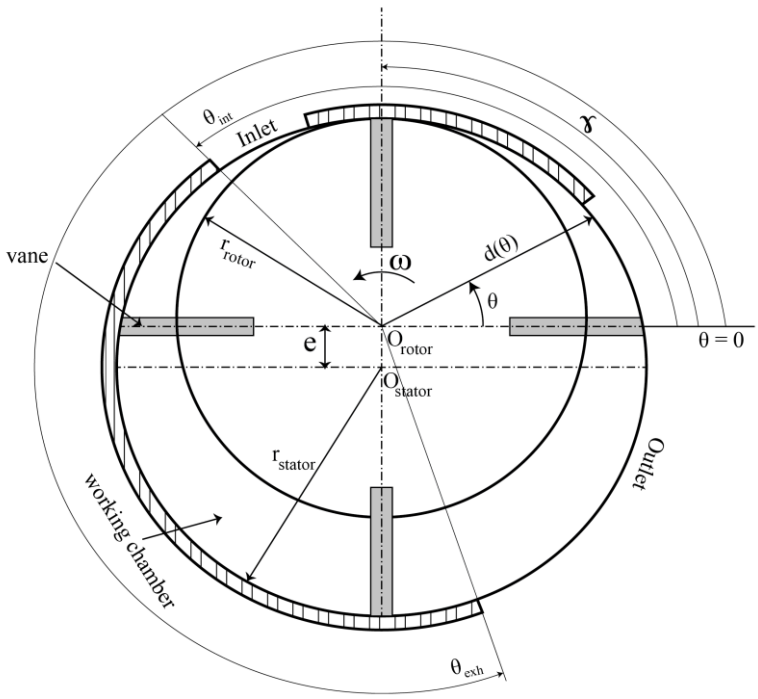

Figure 4 Schematic of the multi-vane expander

In order to evaluate the volume of a working chamber as a function of angular displacement, initially, the radius of the stator to the centre of the rotor is calculated by using the following formula;

$$d(\theta) = -e \times sin\theta + \sqrt{(r_{stat})^2 - (e \times cos\theta)^2} \quad (21)$$

The area of a working chamber can be evaluated if the geometrical parameters of the expander such as stator radius (r_{stat}), rotor radius (r_{rot}), eccentricity (e) and number of the vanes (n) are known.

$$A(\theta) = \frac{1}{2}\int_{\theta}^{\theta+\frac{2\pi}{n}} (d^2 - {r_{rot}}^2)\, d\theta \tag{22}$$

The volume of a working chamber can be given as;

$$V(\theta) = A \times L_{stat} \tag{23}$$

Volume ratio or built-in ratio of an expander can be defined as the ratio between the volume of the working chambers at the end and at the beginning of an expansion process [26]. The volume of the working chambers can be calculated by introducing the intake (θ_{int}) and the exhaust (θ_{exh}) angles into the Eq. (22-23). Thus, built-in ratio is calculated by using the formula below;

$$r_{v,built-in} = \frac{V_{out}}{V_{in}} \tag{24}$$

Following the built-in ratio of the expander, expander designed pressure ratio can be calculated as [27];

$$PR_{dsg} = \frac{P_{exp,in}}{P_{exp,out,dsg}} = \left(r_{v,built-in}\right)^{k_{ratio}} \tag{25}$$

where k represents the heat capacity ratio of the fluid.

As it is stated in [28, 29] that during the expansion process, under-expansion occurs if the designed pressure ratio imposed by the expander is lower than the operating pressure ratio of the system whereas over-expansion happens when the designed pressure ratio is higher than the operating pressure ratio. The operating pressure ratio of the system is the pressure ratio of the collector outlet/expander inlet and expander outlet/condenser inlet.

$$PR_{cyc} = \frac{P_{exp,in}}{P_{exp,out}} \tag{26}$$

Figure 5 represents the isentropic expansion process on a P-V diagram for both under and over expansion cases [29].

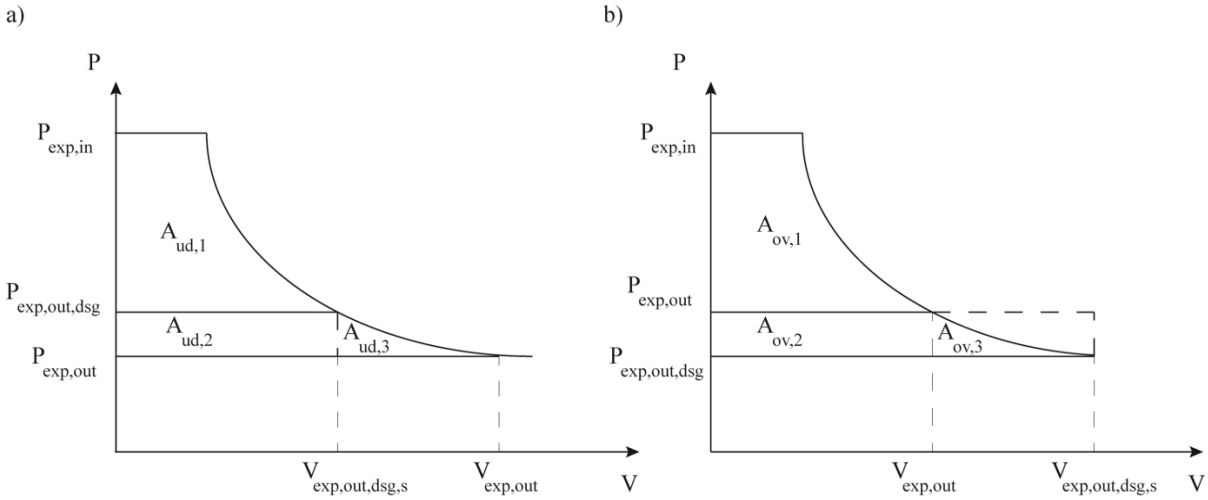

Figure 5 Isentropic expansion process a) under expansion b) over expansion

Then, the work during the expansion process can be calculated according to the areas represented in Figure 5.

Under-expansion

$$\dot{W}_{exp,ud} = A_{ud,1} + A_{ud,2} = \dot{m}_{wf} \times \left(\left(h_{exp,in} - h_{\substack{exp,out \\ dsg,s}} \right) \times 10^{-3} + \left(v_{\substack{exp,out \\ dsg,s}} \times \left(P_{\substack{exp,out \\ dsg}} - P_{exp,out} \right) \right) \times 10^{-2} \right) \times \eta_{mec}$$

(27)

The efficiency of the expander for under-expansion case is calculated as;

$$\eta_{exp,ud} = \frac{\dot{W}_{exp,ud} \times 10^3}{\dot{m}_{wf} \times (h_{exp,in} - h_{exp,out,is})} \tag{28}$$

Over-expansion

$$\dot{W}_{exp,ov} = (A_{ov,1} + A_{ov,2}) - (A_{ov,2} + A_{ov,3}) = \dot{m}_{wf} \times \left(\left(h_{exp,in} - h_{\substack{exp,out \\ dsg,s}} \right) \times 10^{-3} - \left(v_{\substack{exp,out \\ dsg,s}} \times \left(P_{\substack{exp,out \\ dsg}} - P_{exp,out} \right) \right) \times 10^{-2} \right) \times \eta_{mec} \tag{29}$$

The efficiency of the expander for over-expansion case is calculated as;

$$\eta_{exp,ov} = \frac{\dot{W}_{exp,ov} \times 10^3}{\dot{m}_{wf} \times (h_{exp,in} - h_{exp,out,is})} \tag{30}$$

In Eq. (27-30), $h_{exp,in}$ and $h_{exp.out,dsg,s}$ represent the enthalpy at the expander inlet and expander designed outlet isentropic enthalpy respectively. $P_{exp,out,dsg}$ and $P_{exp,out}$ are the designed

expander outlet pressure and expander outlet pressure at operating conditions respectively. $v_{exp,out,dsg,s}$ and η_{mec} indicates expander designed outlet isentropic specific volume and the mechanical efficiency of the expander respectively. Expander mechanical efficiency, which represents the frictional, leakage and heat dissipation losses is assumed to be 0.7 [25].

To validate the expander simulation the model is utilised by using the same expander input conditions as those in [24]; $T_{exp,in}$ = 45.41 ºC, $P_{exp,in}$ = 1.32 bar and $\dot{m}_{wf}$ = 0.022 kg/s. A good agreement between the simulation and experimental results are obtained (Table 1).

Table 1 Expander model validation results

Conditions	**Current study**	**[24]**
$T_{exp,in}$ (ºC)	45.41	45.41
$T_{exp,out}$ (ºC)	36.36	36.36
$P_{exp,in}$ (bar)	1.32	1.32
$P_{exp,out}$ (bar)	0.66	0.66
$\dot{m}_{wf}$ (kg/s)	0.022	0.022
$\dot{W}_{exp}$(W)	**130.3**	**146.74**

2.4. Condenser

The modelled condenser is a water-cooled heat exchanger in which the cooling water circulates to condense working fluid at desired conditions. The condenser is divided into 2 zones during the analysis, which are sensible heat and latent heat rejection respectively. As it is previously mentioned, the working fluid leaves the condenser as saturated liquid at corresponding temperature. The total amount of condensation heat can be calculated as the sum of the sensible and latent heat rejection of the working fluid in the condenser.

$$\dot{Q}_{cond} = \dot{m}_{wf} \times \left(h_{exp,out} - h_{\substack{g@cond \\ temp}} \right) + \dot{m}_{wf} \times \left(h_{\substack{g@cond \\ temp.}} - h_{\substack{l@cond \\ temp.}} \right) \quad (31)$$

The first and the second terms of the right hand side of Eq. (31) represent the sensible and latent heat rejection respectively.

In the condenser modelling, the pinch point temperature (ΔT_{pp}) which is the smallest difference between the working fluid and cooling water temperature is imposed (Figure 6)

[30]. The pinch point (point pp) takes place at where the working fluid starts to condense and the pinch point difference at this point is assumed to be 5 ºC.

$$T_{cond} - T_{cw,pp} \geq \Delta T_{pp} \tag{32}$$

Latent heat rejection represents the enthalpy change of the working fluid from the pinch point to the end of the condenser. This latent heat is equal to the amount of heat that increased the cooling water temperature from the inlet to the pinch point.

$$\dot{m}_{wf} \times \left(h_{\substack{g@cond \\ temp}} - h_{\substack{l@cond \\ temp}} \right) = \dot{m}_{cw} \times C_{p,cw} \times (T_{cw,pp} - T_{cw,in}) \tag{33}$$

As the condensation temperature and the minimum pinch point temperature are defined as 25 ºC and 5 ºC respectively, the cooling water pinch point temperature and the cooling water mass flow rate can be evaluated by utilising Eq. (33) iteratively.

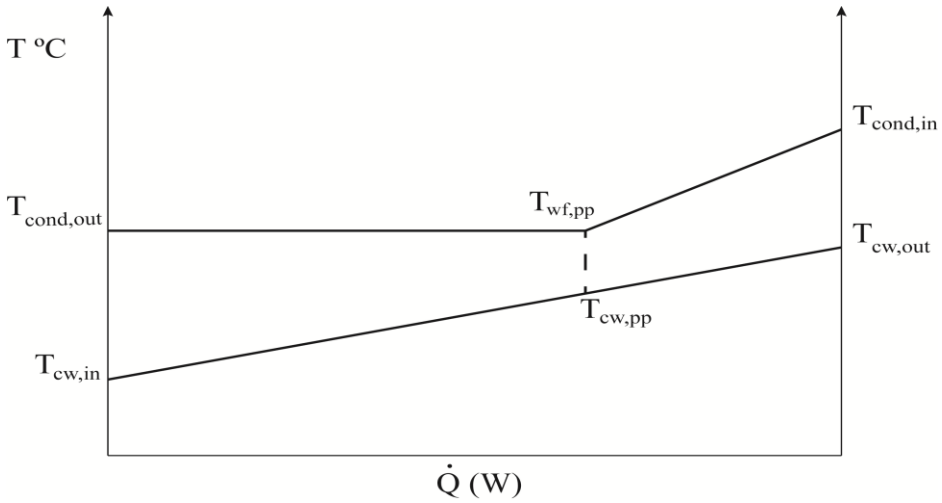

Figure 6 Temperature profiles and the pinch point in the condenser

Then, the cooling water outlet temperature is calculated by using the formula below;

$$\dot{Q}_{cond} = \dot{m}_{cw} \times C_{p,cw} \times (T_{cw,out} - T_{cw,in}) \tag{34}$$

2.5. Pump

The consumed work by the pump is determined by the following equation [31].

$$\dot{W}_{pump} = \frac{\dot{m}_{wf}(v_{pump,in}) \times (P_{evap} - P_{cond}) \times 10^{-2}}{\eta_{pump,s}} \tag{35}$$

where ν is the specific volume of the working fluid, P is the pressure and $\eta_{pump,is}$ is the pump isentropic efficiency. It is important to note that in Eq. (35), the specific volume at the inlet of the pump is used instead of the average of the specific volume at the inlet and outlet of the pump as the difference is small.

3. Numerical process

The simulation model which utilises the developed Matlab computer code is explained in terms of the iteration procedure of the components as well as the whole system in this section. The proposed solar ORC model consists of specific sub-codes which are developed to simulate each component according to the defined input, output and fixed variables. Each component calculates output variables which are utilised as input variables of an another component as each sub-code is connected to each other. In the simulations, the component specifications, the condensing temperature, the ambient and the cooling water temperature, the pump isentropic efficiency, the expander mechanical efficiency and the incoming solar radiation were kept constant whereas the pressure ratio of the cycle was the only selected control variable of the cycle. Properties of each fluid at various operating conditions were taken from REFPROP 9.1 [32] which was developed by the National Institute of Standards and Technology was run in parallel with the computer code. Operating conditions of the system are given in Table 2.

Table 2 Operating conditions of the saturated solar ORC

Parameter	Unit	Value
Incoming solar radiation	W/m^2	800
Condensation temperature	ºC	25
Ambient temperature	ºC	15
Cooling water inlet temperature	ºC	12
Pump isentropic efficiency	-	0.6
Expander mechanical efficiency	-	0.7
Pressure ratio of the cycle	-	1.5 - 6

As the condensing temperature is set constant at 25 ºC, the corresponding condensing pressure at saturated conditions can be determined. The system operating pressure ratio

represents the ratio between the evaporation and the condensation pressure. Thus, the evaporating pressure of each fluid at saturated conditions is determined for each pressure ratio value.

Initially, the fluid properties at given operating conditions is taken from REFPROP (Table 3).

Table 3 Fluid data taken from REFPROP at given operating conditions

Fluid data	
Fluid evaporation temperature at corresponding P_{evap}	Fluid sat. liquid enthalpy at corresponding P_{evap}
Fluid sat. liquid density at corresponding P_{evap}	Fluid sat. vapour enthalpy at corresponding P_{evap}
Fluid sat. liquid density at corresponding P_{evap}	Fluid condensation pressure at 25 ºC
Fluid sat. vapour density at corresponding P_{evap}	Fluid saturated liquid enthalpy at 25 ºC
Fluid sat. liquid conductivity at corresponding P_{evap}	Fluid saturated vapour enthalpy at 25 ºC
Fluid sat. liquid viscosity at corresponding P_{evap}	Fluid saturated liquid specific volume at 25 ºC
Fluid sat. vapour viscosity at corresponding P_{evap}	

As all the necessary fluid data is derived by the computer code, the simulation starts with the determination of the specific pump work by using the following equation;

$$\dot{w}_{pump} = \frac{v_{pump,in} \times (P_{evap} - P_{cond}) \times 10^{-2}}{\eta_{pump,s}} \quad \text{(kJ/kg)} \qquad (36)$$

Thus, the collector inlet enthalpy can be calculated as the pump inlet enthalpy and the pump specific work is known.

$$h_{col,in} = (\dot{w}_{pump} \times 10^3) + h_{pump,in} \quad \text{(J/kg)} \qquad (37)$$

According to the calculated collector inlet enthalpy and given collector (evaporation) pressure, the collector inlet temperature is identified and sent to the computer code.

3.1. Flat plate collector

Previously, a numerical model of the serpentine flat plate collector was developed and experimentally validated [20]. The collector specifications which are also used in this study are given in Table 4.

Table 4 Collector specifications

Collector area (m^2)	6.96
Absorber plate thermal conductivity (W/m-K)	50
Absorber plate thickness (m)	0.001
Total length of tube (m)	56
Tube inner diameter (m)	0.008

Tube outer diameter (m)	0.01
Effective transmittance-absorbance product (-)	0.81

In the model, the collector tube was considered as a single flat tube and was divided into small finite elements. Then, the outlet temperature of the fluid, collector plate temperature, useful heat gain and the collector heat loss at the end of each element and also at the collector outlet was evaluated iteratively for given fluid inlet temperature and fluid mass flow rate. In this study, the same approach is followed by the difference of investigating the mass flow rate for given collector inlet and collector outlet temperature (as the cycle is saturated). Basically, the collector iteration model consists of two parts which are single phase and two phase flow calculations. Single phase flow represents the region from the fluid temperature at the collector inlet to its saturation temperature at corresponding saturation pressure. Two phase flow indicates the region between saturated liquid and saturated vapour points of the fluid. Initially, the simulation considers only the first element in the single phase region and the rest of the elements in the two phase region. Then, after each iteration, the model increases the number of elements in the single phase region until the desired criteria is satisfied. Figure 7 demonstrates the elements and their regions (single or two phase) at two various iteration steps.

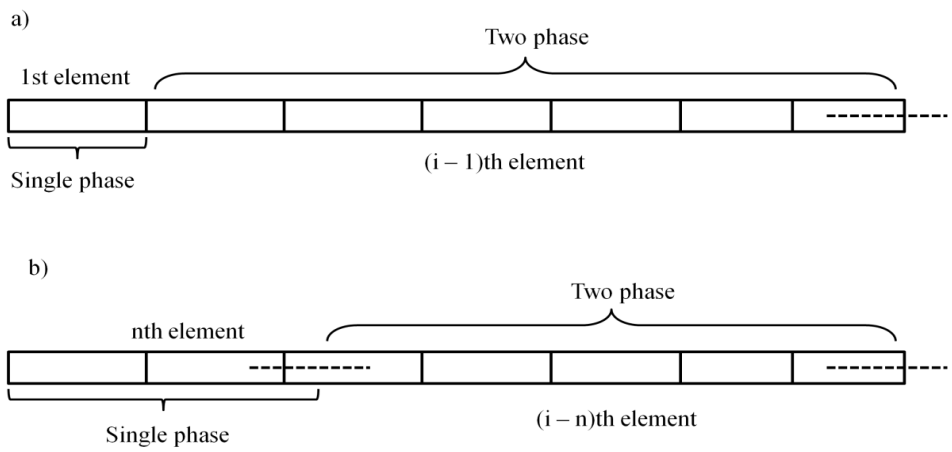

Figure 7 Simulation iteration steps a) first iteration b) xth iteration

At the start, the flow rate of fluid as well as at which element the fluid goes into the saturated region is not known. Therefore, an arbitrary value of the fluid mass flow rate for the first element which represents the single phase flow region is given. Then, in order to calculate the fluid heat transfer coefficient in the single phase region, the flow type is determined whether it is laminar or turbulent by using Eq. (7-8). In the inner loop, the heat loss coefficient is calculated with the given initial plate temperature (T_p) value. (T_p value is considered as 5 °C higher than the fluid inlet temperature for the first iteration) [20]. After the calculation of collector heat loss coefficient, the useful gain of the fluid Q_u is evaluated by using Eq. (3). With the calculated value of Q_u, the new plate temperature is evaluated by using the following equation;

$$T_p = T_{col.in} + \frac{\frac{\dot{Q}_u}{A_p}}{F_R U_T}(1 - F_R) \tag{38}$$

This process is repeated until the difference of two consecutive values of T_p is less than 0.01°C. When the condition of T_p is satisfied in the inner loop, the last value of the useful heat gain of the fluid represents the amount of the heat for the whole collector tube and it can be shown as;

$$\dot{Q}_u = Q_u{}'' \pi D_{in} L_{tube} \tag{39}$$

where $Q_u{}''$ represents the useful heat rate, πD_{in} and L_{tube} indicate the surface perimeter and the length of the collector tube. Then, the heat gain of each element is calculated by using the formula below;

$$\dot{Q}_{gain} = Q_{us}{}'' \pi D_{in} \int_0^L dx \tag{40}$$

In Eq. (40), dx is the length of each element which is obtained by dividing the whole collector tube into ‘n’ number of small elements. Using Eq. (40), the length of the first element is multiplied by useful heat rate and surface perimeter to evaluate the heat gain of the

first element. As the collector inlet temperature and the saturation temperature of the fluid is known, the amount of the sensible heat transfer can be calculated as;

$$\dot{Q}_{snb} = \dot{m}_{wf,sp} \times C_p \times \left(T_{evap} - T_{col,in}\right) \tag{41}$$

Then, the mass flow rate for single phase flow is calculated as the sensible heat transfer is equal to the heat gain of the first element.

$$\dot{m}_{wf,sp} = \frac{\dot{Q}_{gain,sp}}{C_p \times \left(T_{evap} - T_{col,in}\right)} \tag{42}$$

New calculated mass flow rate value of the fluid in the single phase region indicates that the first iteration assumes that the fluid undergoes a phase change in other words reaches its saturation points after the first element with the calculated mass flow rate. Then, the second loop starts where the two phase flow calculations are performed. In this loop, again the heat loss coefficient is evaluated by using the latest calculated T_p value. The useful heat gain of the fluid is evaluated (Eq. (3)) with another arbitrary value of the fluid mass flow rate for two phase region. Similar to the single phase part of the code, the new plate temperature is evaluated with the calculated value of useful heat (Eq. (38)). The process is repeated until the same convergence criterion is met (0.01°C). Then, the heat gain of the fluid for the rest of the collector elements is calculated again by using Eq. (39). Differently from the first part, useful heat rate and surface perimeter are multiplied by another figure which equals to the length of the first element subtracted from the total length of the tube. Then, similarly like the sensible heat, the amount of the latent heat transfer can be calculated as;

$$\dot{Q}_{lat} = \dot{m}_{wf,tp} \times \left(h_g - h_l\right) \tag{43}$$

and the mass flow rate for the two phase region;

$$\dot{m}_{wf,tp} = \frac{\dot{Q}_{gain,tp}}{\left(h_g - h_l\right)} \tag{44}$$

At the end of the second loop, the model checks if the difference between $\dot{m}_{wf,sp}$ and $\dot{m}_{wf,tp}$ is less than 0.0001. If the condition does not meet the convergence criterion (0.0001), the

model increases the number of elements for the single phase part region and the same calculations are performed. This is continued until the condition satisfies the convergence. This point represents the element where the flow reaches the saturation point with corresponding mass flow rate. Finally, the collector efficiency is determined as;

$$\eta_{col} = \frac{\dot{m}_{wf} \times \left[\left(C_p\left(T_{evap} - T_{col,in}\right) + \left(h_g - h_l\right)\right)\right]}{S \times A_{col}} \tag{45}$$

The flow chart of the simulation model is represented in Figure 8.

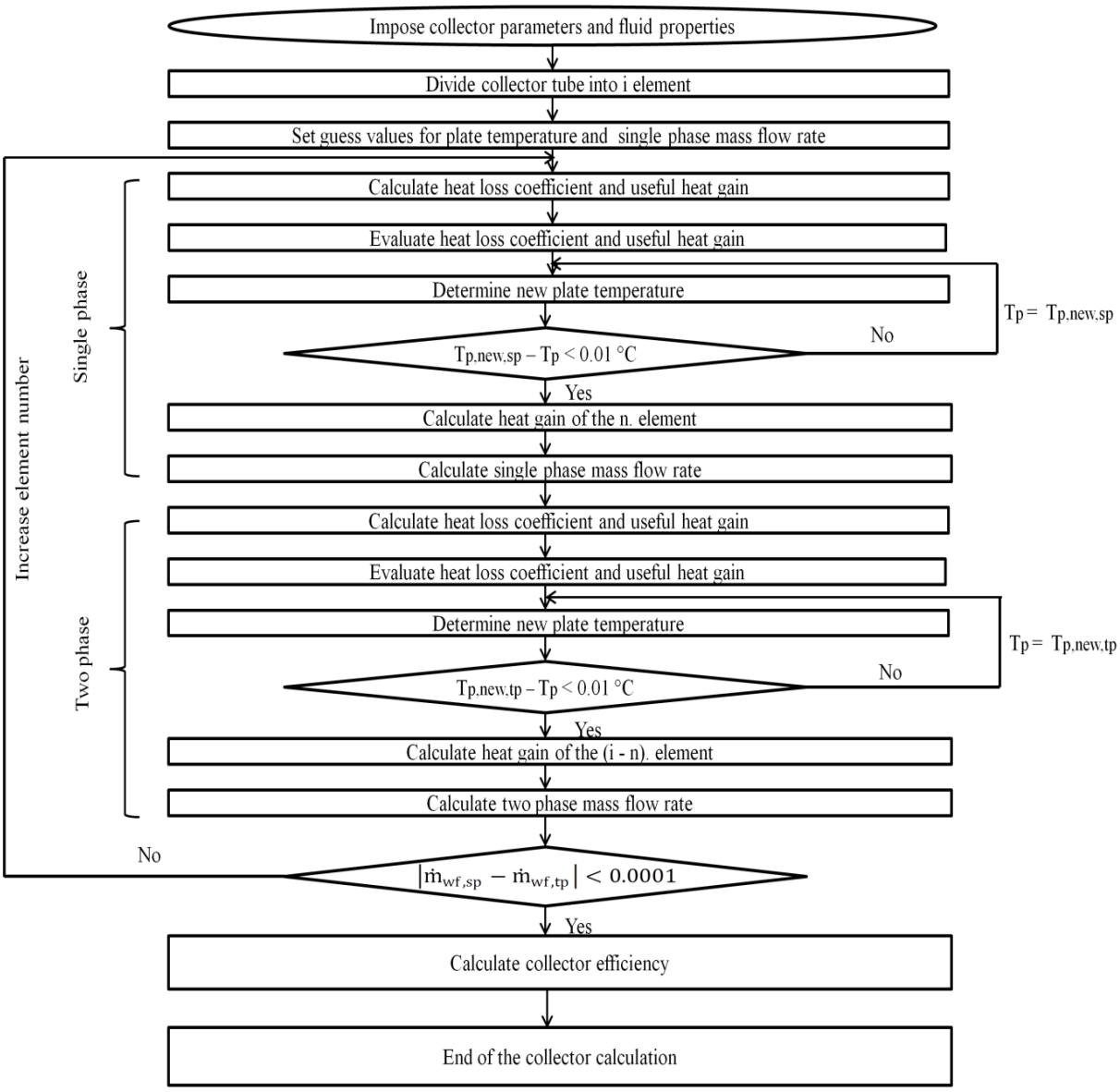

Figure 8 Flow chart of the simulation model

3.2. Expander

The iteration begins with setting the parameters and the inputs of the expander. The parameters of the expander, inputs and outputs of the expander model are given in Table 5. Then the expander built-in ratio and expander designed outlet pressure are calculated by using Eq. (24-25). As it is previously mentioned, the fluid at the inlet of the expander is saturated vapour at corresponding evaporation pressure. This means the entropy at the outlet of the expander is equal to the entropy at the inlet of the expander as long as the expansion process is isentropic. Therefore, at the given entropy and expander designed outlet pressure, expander designed outlet isentropic enthalpy and isentropic specific volume can be calculated.

Table 5 Expander model specifications

Parameters	**Inputs**	**Outputs**
Rotor radius, (r_{rot})	Inlet pressure, ($P_{exp,in}$)	Built-in volume ratio, ($r_{v,built\text{-}in}$)
Stator radius, (r_{stat})	Outlet pressure, ($P_{exp.out}$)	Expander designed outlet pressure, ($P_{exp,out,dsg}$)
Eccentricity, (e)		Expander designed outlet isentropic enthalpy, ($H_{exp,out,dsg,s}$)
Intake angle, (θ_{int})		Expander designed outlet isentropic specific volume, ($v_{exp,out,dsg,s}$)
Exhaust angle, (θ_{exh})		Expander mechanical work, ($\dot{W}_{exp}$)
Expander mechanical efficiency, (η_{mec})		Expander efficiency, (η_{exp})

As all the unknowns in Eq. (27-30) are evaluated, now the model compares the designed and system operating pressure ratio values. Then, the mechanical work generated in the expander and the expander efficiencies are calculated according to the conditions of under and over expansion. The flow chart of the expander model is given in Figure 9.

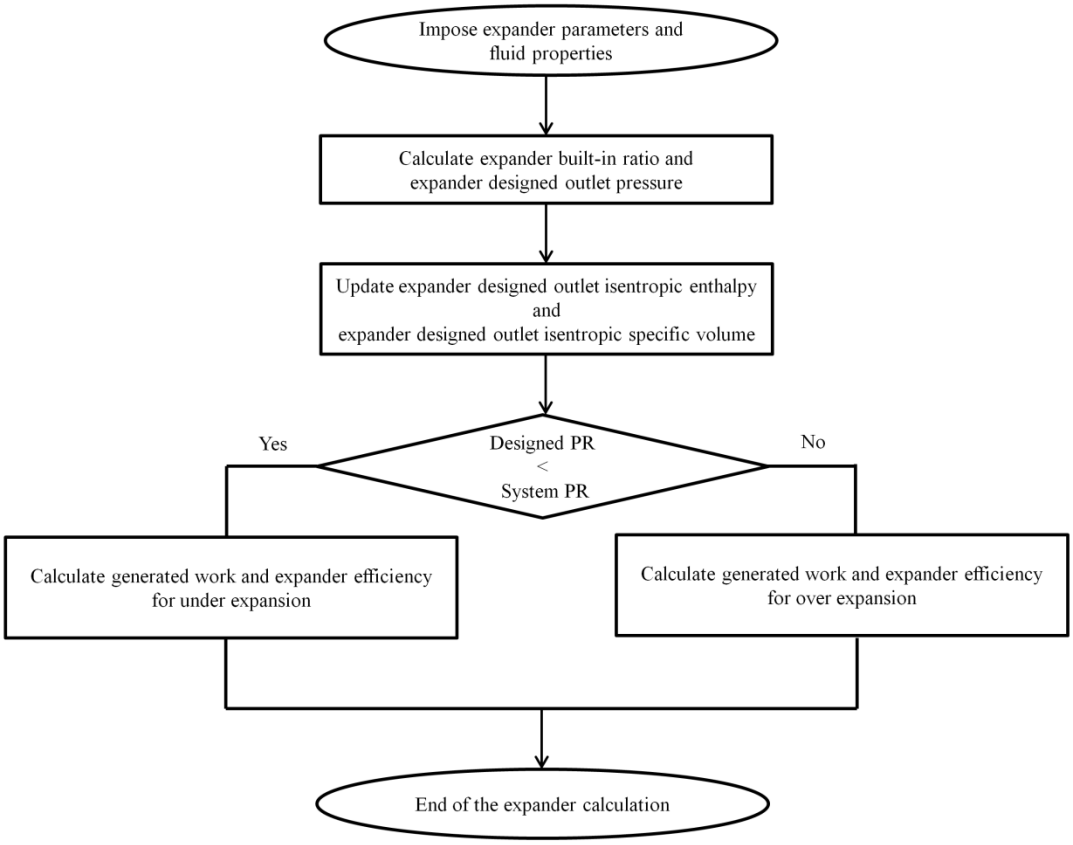

Figure 9 Flow chart of the expander simulation model

3.3. Condenser

In the condenser simulations, cooling water mass flow rate and outlet temperature are aimed to be determined. Initially, pinch point condition in the code is set as;

$$25 - T_{cw,pp} \geq 5\ °C \tag{46}$$

This is to evaluate the cooling water mass flow rate. Then, with the given initial cooling water mass flow rate (0.001 kg/s), cooling water pinch point temperature is calculated by using Eq. (33) iteratively where the mass flow rate is increased by 0.001 intervals until the condition (Eq. 46) is satisfied. This point provides the real value of the cooling water mass flow rate and cooling water pinch point temperature. Thereafter, the cooling water outlet temperature is evaluated with the use of Eq. (34) as the cooling water mass flow rate is determined previously. It is important to note that Eq. (31) is valid as long as the fluid leaves the expander as superheated vapour. However, if the fluid falls in the saturation region after

the expansion process, the first term of the right hand side of Eq. (31) which represents the sensible heat rejection is omitted and the following equation is utilised to calculate the total amount of the condensation heat.

$$\dot{Q}_{cond} = \dot{m}_{wf} \times \left(h_{exp,out} - h_{\substack{l@cond \\ temp}} \right) \tag{47}$$

As the sensible heat rejection does not occur, the smallest difference between the working fluid and cooling water temperature takes place at the point where the cooling water leaves the condenser. Therefore, Eq. (33) can be rewritten as:

$$\dot{m}_{wf} \times \left(h_{exp,out} - h_{\substack{l@cond \\ temp}} \right) = \dot{m}_{cw} \times C_{p,cw} \times (T_{cw,out} - T_{cw,in}) \tag{48}$$

Then, Eq. (48) is solved iteratively with the same condition (Eq. 46) to calculate the cooling water mass flow rate and outlet temperature.

3.4. The saturated solar ORC

The model of the whole solar ORC is developed by interconnecting all the components with the given input parameters. The performance analysis of the cycle is evaluated through the performance parameters.

The first performance parameter is the net work output of the system and it is defined as;

$$\dot{W}_{net} = \dot{W}_{exp} - \dot{W}_{pump} \tag{49}$$

The other parameter is the solar ORC efficiency and it is calculated as;

$$\eta_{SORC} = \frac{\dot{W}_{net} \times 10^3}{\dot{Q}_{gain}} \tag{50}$$

3.5. Simulation model constraints

The boundary conditions of the saturated solar ORC model are listed below;

- Superheating at the expander inlet and sub-cooling at the condenser outlet are zero, in other words working fluid leaves the collector as saturated vapour and leaves the condenser as saturated liquid in order to reduce total irreversibility of the cycle [33] .

- The saturated solar ORC is simulated at a constant condensing temperature of 25 ºC
- As the fluids undergo a phase change in the collector, the maximum pressure of the cycle is limited to 1.5MPa (15 bar) due to the leakage and safety concerns of the maximum flat plate collector pressure in domestic applications.
- Minimum condenser pressure should be higher than 0.05 bar [34].
- Pump isentropic efficiency is 0.6 [35].

3.6. Fluid pre-selection

In order to narrow down the list of the potential candidates to be used in the proposed solar ORC, some of the compounds were eliminated, according to their environmental parameter (ODP) and their corresponding saturation pressure at 25 ºC in the condenser. Several Hydrocarbons and Siloxanes have been discarded from the analysis due to having corresponding condensation pressure less than 0.05 bar at 25 ºC (Table 6).

Table 6 Fluids with a condensation pressure less than 0.05 bar

Fluid	**Condensation pressure at 25 ºC (bar)**
D4	0.0012
Decane	0.001
Dodecane	0.0001
Ethyl benzene	0.012
MDM	0.004
MD2M	0.0005
MD3M	0.00006
m-xylene	0.011
Nonane	0.005
Octane	0.018
p-xylene	0.011
Toluene	0.037

Table 7 Properties of the investigated fluids [32]

Fluid	Alt. Name	Type	T_{crit} (ºC)	P_{crit} (bar)	$T_{boiling}$ (ºC)*	Molar Mass (kg/kmol)
Trans-2-butene		HC	155.46	40.27	0.88	56.106
Cis-2-butene		HC	162.6	42.25	3.72	56.106
1-butene		HC	146.14	40.05	-6.31	56.10
Isobutane	R600a	HC	134.66	36.29	-11.74	58.122
Butane	R600	HC	151.98	37.96	-0.49	58.122
Neopentane		HC	160.59	31.96	9.5	72.149
Isopentane	R601a	HC	187.2	33.78	27.83	72.149
Pentane	R601	HC	196.55	33.7	36.06	72.149
Isohexane		HC	224.55	30.4	60.21	86.175
Hexane		HC	234.67	30.34	68.71	86.175
Cyclohexane		HC	280.45	40.805	80.71	84.159
1,1,1,2-tetrafluoroethane	R134a	HFC	101.06	40.593	-26.07	102.03
1,1-difluoroethane	R152a	HFC	113.26	45.168	-24.02	66.05
1,1,1,2,3,3,3-heptafluoropropane	R227ea	HFC	101.75	29.25	-16.34	170.03
1,1,1,2,3,3-hexafluoropropane	R236ea	HFC	139.29	34.2	6.17	152.04
1,1,1,3,3,3-hexafluoropropane	R236fa	HFC	124.92	32.0	-1.49	152.04
1,1,1,3,3-pentafluoropropane	R245fa	HFC	154.01	36.51	15.14	134.05
1,1,2,2,3-pentafluoropropane	R245ca	HFC	174.42	39.40	25.26	134.05
Octafluorocyclobutane	RC318	PFC	115.23	27.775	-5.97	200.03
Methyl-heptafluoropropyl-ether	RE347mcc	HFE	164.55	24.762	34.19	200.05
2,2,2-trifluoroethyl-difluoromethyl-ether	RE245fa2	HFE	171.73	34.33	29.25	150.05
2,3,3,3-Tetrafluoropropene	R1234yf	HFO	94.7	33.82	-29.45	114.04
Trans-1,3,3,3-tetrafluoropropene	R1234ze	HFO	109.36	36.34	-18.97	114.04
Trans-1-chloro-3,3,3-trifluoropropene	R1233zd	HFO	165.6	35.70	18.32	130.5

* Normal boiling temperature at 1 bar

Ozone depletion potential (ODP) states compound's potential to contribute ozone degradation is one of the vital environmental factors for working fluid selection [34, 36]. Due to their high ODP values Chlorofluorocarbons (CFCs) and hydrochlorofluorocarbons (HCFCs) are discarded from the analysis. Thus, the fluids belong to Hydrocarbons (HCs), Hydrofluorocarbons (HFCs), Perfluorocarbons (PFCs), Hydrofluoroolefins (HFOs) and Hydrofluoroethers (HFEs) are considered and analysed in this study and 24 fluids given in Table 7 are considered as potential candidates.

4. Results and discussion

In this section, the simulation results of the proposed saturated solar ORC at various pressure ratio using 24 working fluids are presented. It is well known that the net work output and the thermal efficiency of an ORC increase with the increasing difference of condenser

and evaporator pressure and temperature. However, as it is previously stated, the flat plate collector is utilised as the evaporator (heat source) of the cycle in this study and the collector efficiency, in other words the amount of the heat that is recovered by the working fluid in the collector is highly related to the collector temperature due to the heat losses to the atmosphere as the collector efficiency is not set constant. Furthermore, unlike many studies in the literature, turbine/expander efficiency was not fixed and it varied as the expander inlet pressure changes due to the different behaviours of expansion (under/over) losses in the expander. Therefore, special attention is given to the collector and expander characteristics under various pressure ratio values of the system when the whole system is analysed in this section.

As it is stated previously, the maximum collector pressure is set to 15 bars. However, fluids such as R-134a, R-152a, R-227ea, R-236fa, RC-318, 1-butene, R-600a and RE-170 have an evaporation/collector pressure greater than 1.5 MPa at some pressure ratio points. This is due to their low saturation temperature behaviours. In the analysis, only the cases where the evaporation pressure is less than 1.5MPa ±0.75 is taken into account for these fluids (Table 8).

Table 8 Fluid corresponding evaporation pressures at various pressure ratio values

Fluid	**Pressure Ratio**										
	P_{cond} at 25 ºC (bar)	1.5	2	2.5	3	3.5	4	4.5	5	5.5	6
1-butene	2.95	4.43	5.91	7.39	8.87	10.35	11.83	13.31	14.79	**16.27**	**17.75**
R-600a	3.49	5.23	6.98	8.72	10.47	12.21	13.96	15.71	**17.45**	**19.20**	**20.94**
R-134a	6.62	9.93	13.2	**16.56**	**19.87**	**23.18**	**26.49**	**29.80**	**33.12**	**36.43**	**39.74**
R-152a	5.93	8.90	11.8	14.84	**17.81**	**20.78**	**23.75**	**26.71**	**29.68**	**32.65**	**35.62**
R-227ea	4.52	6.78	9.05	11.31	13.57	15.84	**18.10**	**20.36**	**22.63**	**24.89**	**27.15**
R-236fa	2.7	4.05	5.41	6.76	8.11	9.47	10.82	12.17	13.52	14.88	**16.23**
RC-318	3.11	4.66	6.22	7.77	9.33	10.88	12.44	13.99	15.55	**17.10**	**18.66**
R1234yf	6.79	10.1	13.5	**16.9**	**20.3**	**23.78**	**27.18**	**30.5**	**-**	**-**	**-**
R1234ze	4.96	7.44	9.92	12.4	14.88	**17.36**	**19.85**	**22.33**	**24.81**	**27.29**	**29.77**

4.1. Collector analysis

The efficiency of the collector for each fluid category (HC, HCF, PFC, HFE and HFO) at various pressure ratios is represented in Figure 10. It can be seen that the collector efficiency decreases independently of the fluid category as the pressure ratio of the system increases. This can be explained by the fact that the higher pressure ratio leads to an increase in the saturation pressure, as well as saturation temperature in the collector (saturated ORC). As a result, higher collector temperature causes greater heat loss from the collector to the ambient [16, 20].

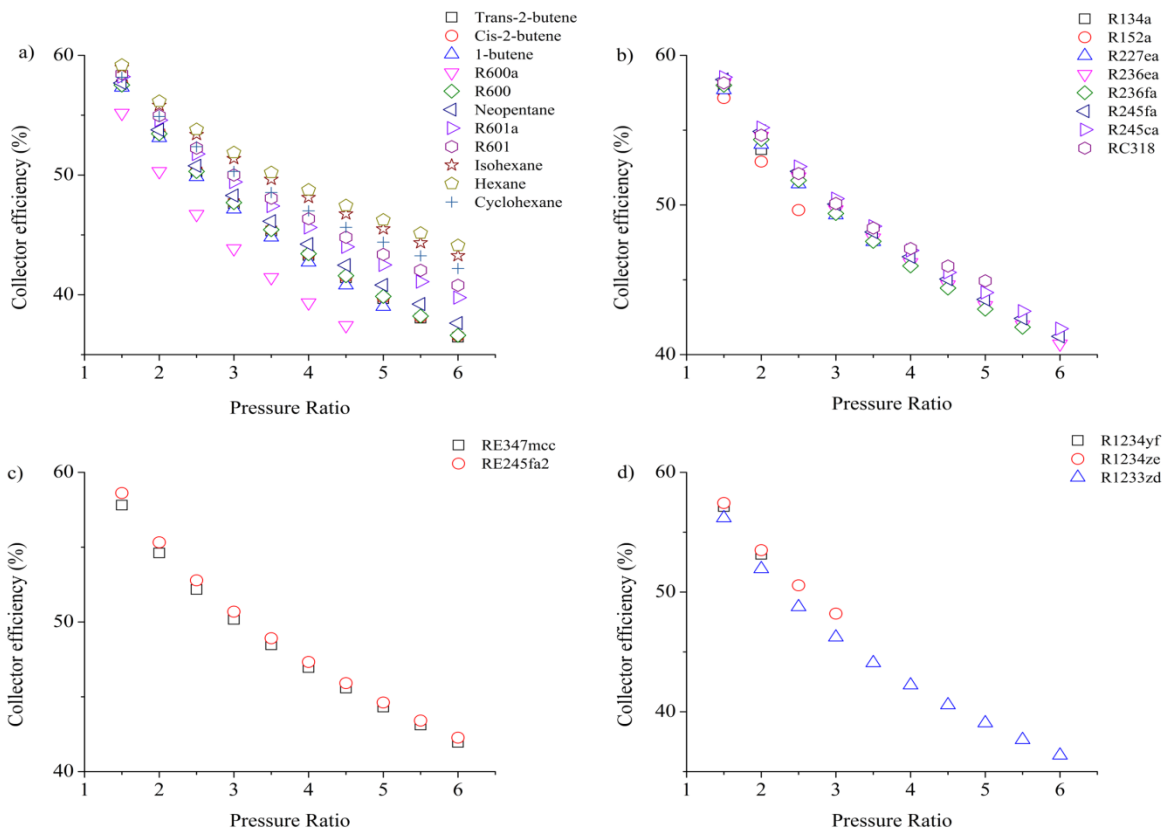

Figure 10 Collector efficiency a) HCs b) HFC-PFCs c) HFEs d) HFOs

Figure 11 shows the collector heat loss and the saturation temperature of the fluids R600a, R236ea, RE245fa2 and R1234ze as an example. In general, the collector efficiency for all the investigated fluids varied between 59.19% and 37.44% and the highest and the lowest efficiency value is obtained from Hexane and R-600a which ranged from 59.19% to 44.12% and 55.18% to 37.44% respectively.

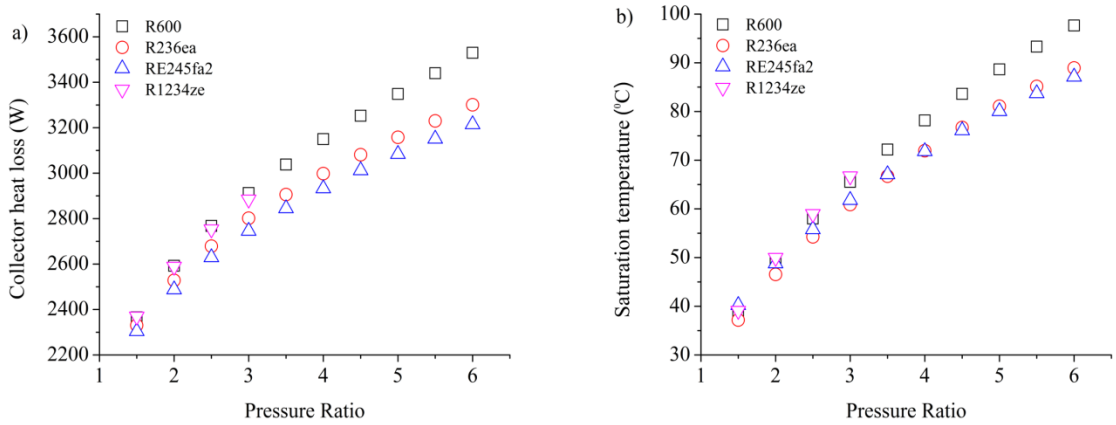

Figure 11 Collector heat loss and saturation temperature with pressure ratio

4.2. Expander analysis

In this section, the vane expander efficiency is analysed in terms of investigating the relation between the expander designed pressure ratio PR_{dsg} and the system pressure ratio PR_{cyc}. It can be seen from Figure 12 that for each investigated fluid, the maximum expander efficiency occurred at the pressure ratio of 2.5 which also represents the designed expander pressure ratio (PR_{cyc}). The only exception was R134a and R1234yf where the pressure ratio of 2 provides the highest efficiency due to their saturation pressure limitation.

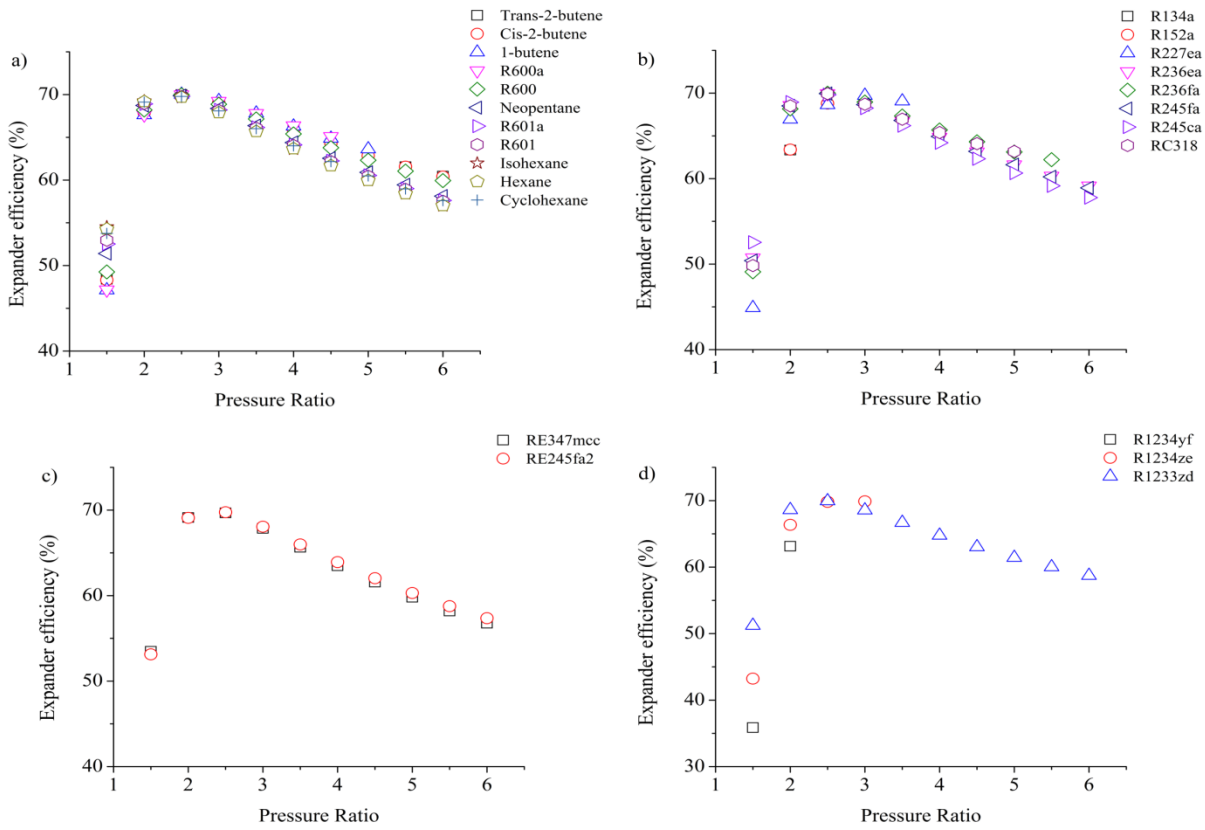

Figure 12 Expander efficiency under various pressure ratio a) HCs b) HFC-PFCs c) HFEs d) HFOs

For instance, the efficiency of R600 was to be 49.26% at a pressure ratio of 1.5 which is lower than its designed pressure ratio and results in over-expansion. Then, the efficiency increases to 68.2% as the pressure ratio rises to 2 and the efficiency reaches its maximum (69.98%) at PR of 2.5. After η_{exp} achieves the maximum value, it decreases gradually with increasing pressure ratio. This is because further increase in PR causes the expander to operate under the under-expansion zone.

The minimum expander efficiency (35.61%) is obtained from the pressure ratio of 1.5 with R134a and the maximum expander efficiency (70.1%) is observed for the pressure ratio of 2.5 with 1-butene among the considered fluids. It is important to note that the analysis shows that the design parameters of a vane expander and the operating parameters of the cycle has a significant influence on the expander performance as it is also stated by [25, 29]. It is also worth mentioning that all the investigated fluids except HFC-152a left the expander as a superheated vapour which shows that there is no risk of encountering any liquid droplet in the

expander. The only exception was HFC-152a which was in the superheated vapour region at the pressure ratio of 1.5, then fell into the saturated region and had vapour quality of 0.997, 0.988 and 0.982 at the pressure ratio of 2, 2.5 and 3 respectively. Thereby, superheating might be necessary when utilising HFC-152a in order to avoid liquid formation in the expander.

4.3. Condenser analysis

It was previously mentioned that the heat rejection from the proposed cycle was carried out in the condenser. The working fluid was cooled by water which has an inlet temperature of 12 °C. The amount of the calculated condensation heat varied between 1729 W and 3223.96 W. Thus, this amount of heat was transferred from the system to the cooling water which subsequently increased the water temperature at the outlet of the condenser. The cooling water mass flow rate and the cooling water temperature at the exit of the condenser was calculated for each considered fluid. The results at pressure ratio of 1.5 are represented in Table 9. As it can be seen from Table 9 that the cooling water mass flow rate varied from 0.087 kg/s to 0.094 kg/s and the cooling water outlet temperature varied between 18.65 °C and 20.45 °C. Furthermore, the increased temperature of cooling water at the collector outlet can be utilised for secondary uses. For instance, the cooling water flow can be directed to a hot water tank to recover some portion of its heat [24].

Table 9 Calculated cooling water mass flow rate and outlet temperature at pressure ratio of 1.5

Fluid	Cooling water mass flow rate (kg/s)	Cooling water inlet temperature (°C)	Cooling water outlet temperature (°C)
Trans-2-butene	0.091	12	20.21
Cis-2-butene	0.092	12	20.11
1-butene	0.091	12	20.16
R600a	0.087	12	20.25
R600	0.091	12	20.14
Neopentane	0.09	12	20.33
R601a	0.092	12	20.16
R601	0.093	12	20.14
Isohexane	0.094	12	20.18
Hexane	0.094	12	20.2
Cyclohexane	0.094	12	19.99
R134a	0.093	12	20.13
R152a	0.093	12	20
R227ea	0.09	12	20.39
R236ea	0.092	12	20.22
R236fa	0.092	12	20.23
R245fa	0.093	12	20.18
R245ca	0.093	12	20.18
RC318	0.09	12	20.45
RE347mcc	0.091	12	20.43
RE245fa2	0.093	12	20.23
R1234yf	0.091	12	19.01
R1234ze	0.091	12	20.24
R1233zd	0.09	12	18.65

4.4. Solar ORC analysis

In this section the net work output of the cycle with the thermal efficiency of the solar ORC is investigated. Figure 13 shows the net work output of the cycle for each investigated fluid. It can be observed that the net work output of the cycle augments initially, reaches its peak and remains almost constant with the increasing pressure ratio for 1-butene, R600a, hexane, Isohexane, Cyclohexane, R236fa, R245fa and RE245fa2.

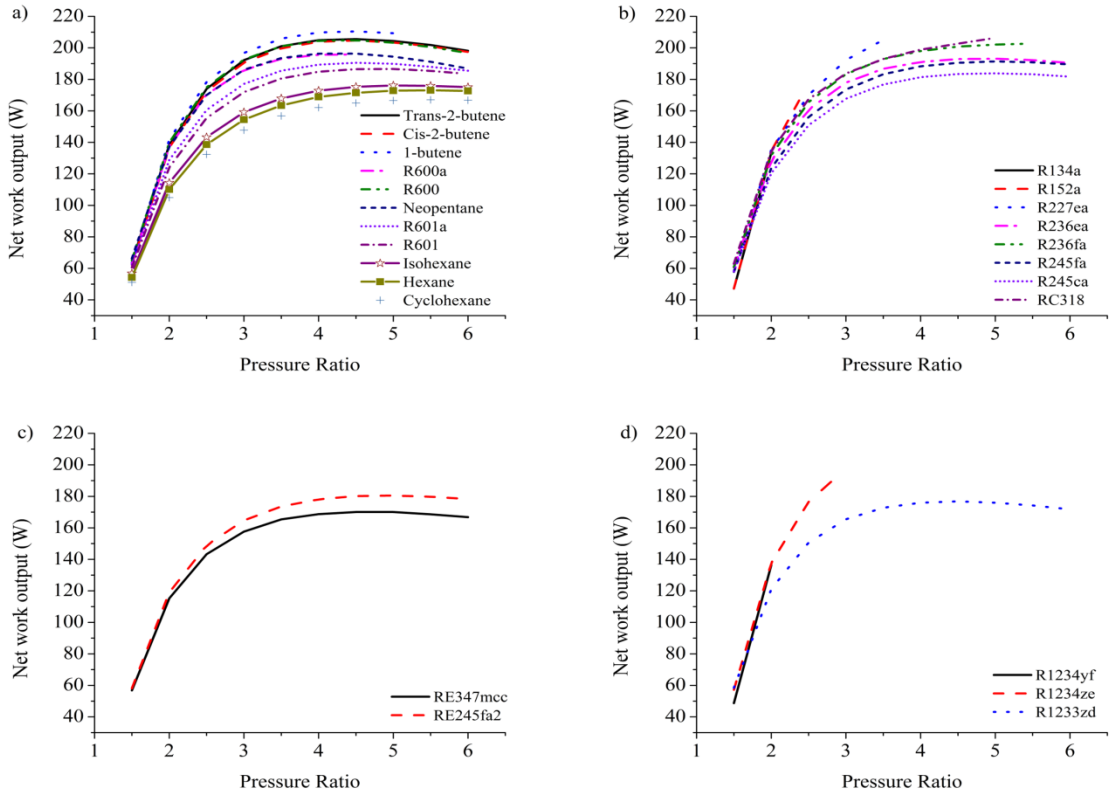

Figure 13 Net work output versus pressure ratio for a) HCs b) HFC-PFCs c) HFEs d) HFOs

The reason for this behaviour can be explained by the decrease in the mass flow rate of the cycle and increase in the consumed pump work. The former is due to the rise in the pressure ratio of the system at a constant condensation pressure, which augments the difference between the collector and condenser pressure that represent the highest and the lowest points of the cycle respectively. This results in an increase in the enthalpy difference between the two points and causes the mass flow rate to decrease due to the energy balance of the cycle. Figure 14 represents the mass flow rate of four working fluids versus pressure ratio as an example.

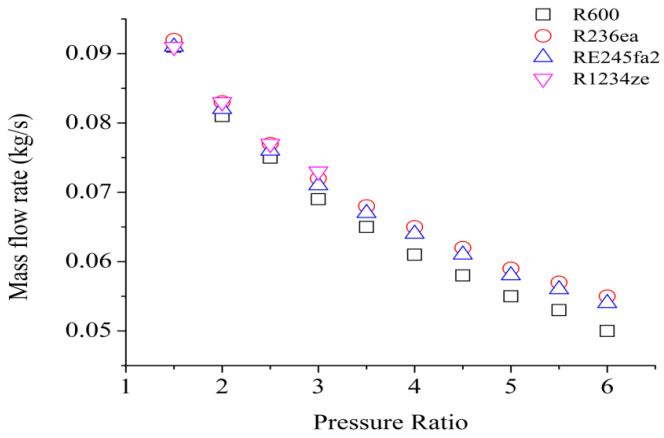

Figure 14 Mass flow rate of R600, R236ea, RE245fa2 and R1234ze versus pressure ratio

It can be observed that initially, the effect of the increase in the enthalpy drop across the expander is higher than the decrease in the mass flow rate and the increase in the consumed pump work. However, after a certain point of the pressure ratio the increase in the enthalpy drop does not dominate the decrease in the mass flow rate and the rise in the consumed pump work. This is even more pronounced for the fluids such as trans-2-butene, cis-2-butene, R600, neo-pentane, R601a, R236ea, R245ca, RE347mcc and R1233zd where the net work output starts to decline beyond the pressure ratio of the maximum net work output. The same trend can be found in [17, 30]. On the other hand, fluids such as R134a, R152a, R227ea, RC318, R1234yf, R1234ze shows an increasing tendency with the rising pressure ratio owing to the limitations of their saturation pressure points higher than 15 bars.

Another parameter which is investigated in this section is the thermal efficiency of the solar ORC. As it is stated by [14] it is important to consider net work output along with the thermal efficiency when comparing various working fluids. It is apparent from Figure 15 that the cycle efficiency increases with increasing pressure ratio for each investigated fluid. Similar trend can be found in [19].

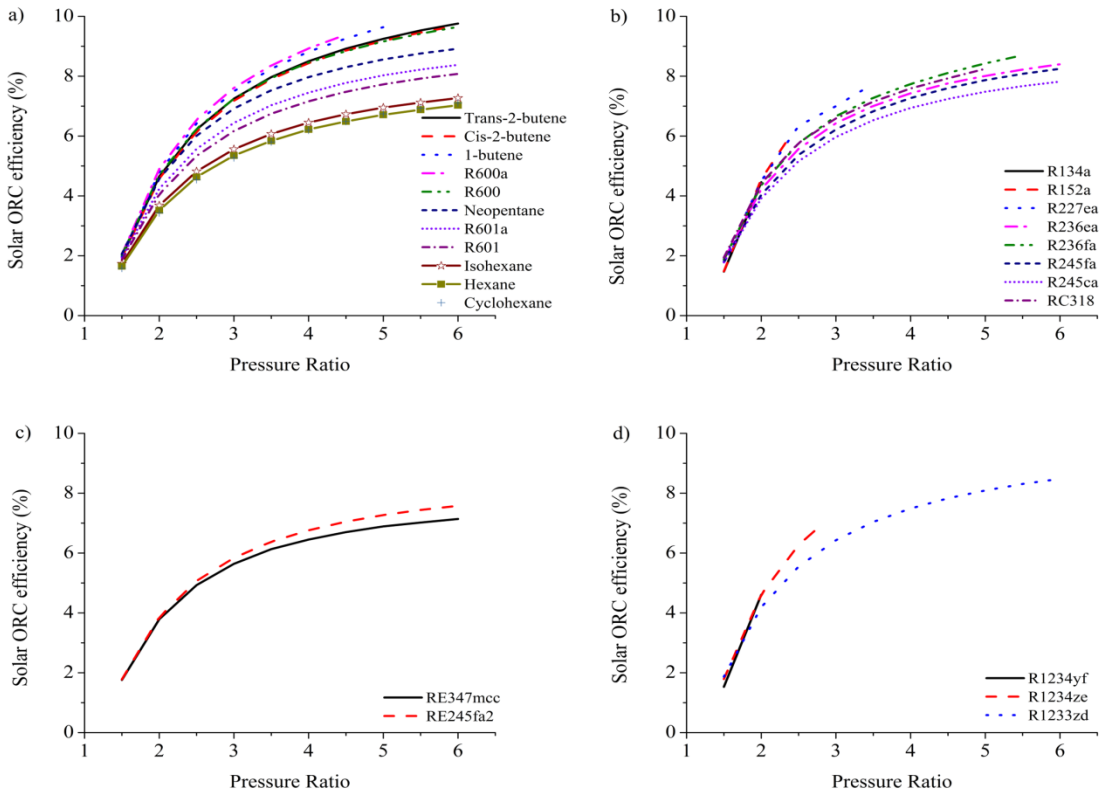

Figure 15 Solar ORC efficiency varies with pressure ratio for a) HCs b) HFC-PFCs c) HFEs d) HFOs

This behaviour is different from the net work output of the cycle as it is demonstrated previously in Figure 13. The reason for the upward trend of cycle efficiency when there is a maximum point for the net work output is the decrease in the amount of the heat gained by the fluid in the collector. Similar results were reported in [33] for R134a refrigerant. The highest cycle efficiency is obtained by trans-2-butene (9.76%) and cis-2-butene (9.69%) among the investigated fluids.

Figure 13 and Figure 15 represents that generally, HCs provide higher net work output and cycle efficiency compared to the others thermofluids and among the hydrocarbons, trans-2-butene, cis-2-butene, 1-butene, R600 and R600a gives the highest results. For HCFs, HFEs and HFOs R227ea, R236fa, RC318 and R1234ze generate more net power output, whereas R227ea, R236ea, R236fa and RC318 provide higher thermal efficiency.

It is important to note that the net mechanical work output of R236ea (60.57W-190.39W) is found to be less than R227ea (58.18W-205.06W) and RC318 (62.94W-206.34W). However,

the cycle efficiency of R236ea (1.87%-8.4%) is greater that of R227ea (1.81%-7.75%) and RC318 (1.94%-8.25). This can be explained by the fact that R236ea provides less collector efficiency (58.15%-40.72%) compared to R227ea (57.69%-47.57%) and RC318 (58.16%-44.93%). In other words, less amount of useful heat is transferred to R236ea owing to its higher saturation (collector) temperature. According to Eq. (50), the higher cycle efficiency of R236ea shows an interesting potential of converting the heat energy into the mechanical work.

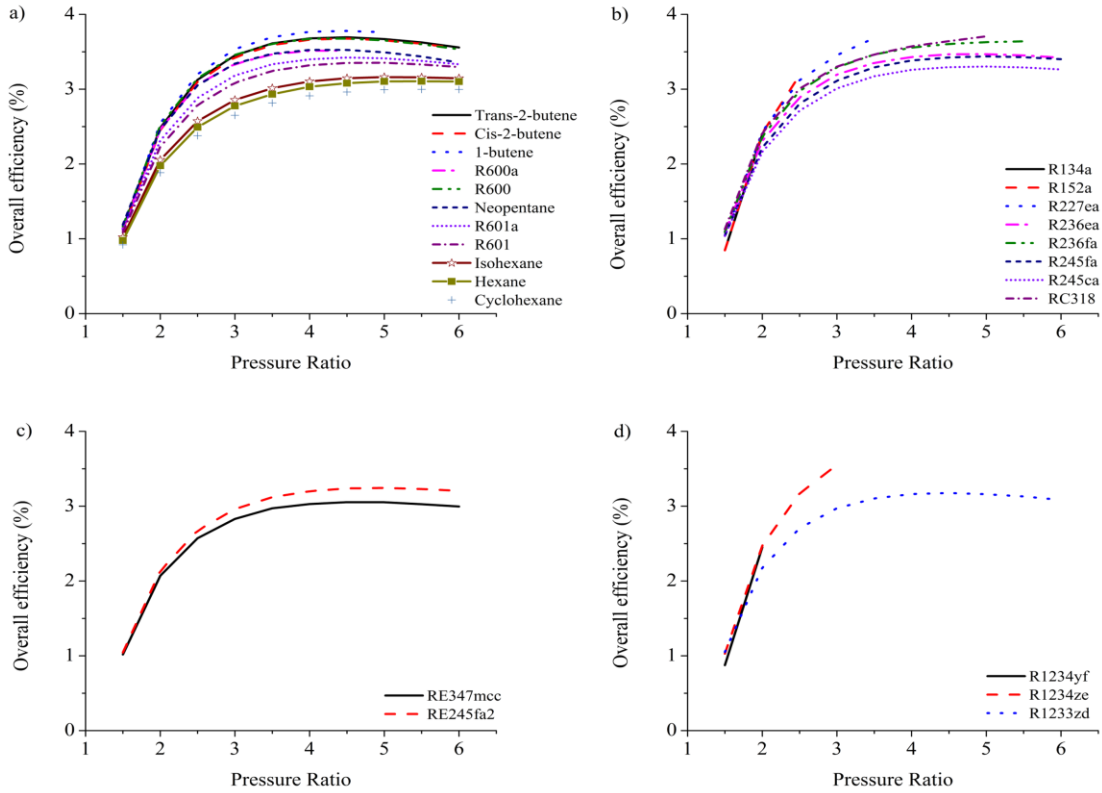

Figure 16 Overall efficiency varies with pressure ratio for a) HCs b) HFC-PFCs c) HFEs d) HFOs

In addition to the thermal efficiency of the proposed solar ORC, the overall efficiency which represents the ratio of the net power output of the cycle to the incoming solar radiation is calculated as:

$$\eta_{sys} = \frac{\dot{W}_{net}}{SA_{col}} \tag{51}$$

The overall efficiency shows similar trend with the net work output of the solar ORC (Figure 16). The highest overall efficiency is obtained by 1-butene (3.78 %) and this is followed by trans-2-butene (3.69%) and cis-2-butene (3.72%).

4.5. Environmental and safety impacts

In this section, the environmental impact of the fluids in terms of the contribution to the global warming and the safety characteristics of the fluids such as flammability and toxicity are discussed and the properties of the fluids are given in Table 10. It can be seen from Table 10 that some refrigerants such as HFCs and PFC have considerably high global warming potential. As an example, R236fa and RC318 have a GWP of 6300 and 10300 respectively. On the other hand, HFEs, HFOs and HCs have a negligible global warming potential [37-39]. Another environmental concern of the fluids is the flammability and toxicity. Hydrocarbons are more flammable compared to the other fluid categories such as HFCs, HFEs and HFOs.

4.6. Overall analysis of the thermofluids

In general, as it is stated by several researchers there is no fluid which can satisfy all the conditions such as providing high thermal efficiency and net work output, having reasonable saturation points and low GWP and being non-flammable [19, 28].

Table 10 Environmental and safety data of the considered fluids

Fluid	Alt. Name	Type	GWP	Safety
Trans-2-butene		HC	~20 [33]	-
Cis-2-butene		HC	~20 [33]	-
1-butene		HC	~20 [33]	-
Isobutane	R600a	HC	~20 [33]	A3 [19]
Butane	R600	HC	~20 [33]	A3 [19]
Neopentane		HC	~20 [33]	-
Isopentane	R601a	HC	~20 [33]	A3 [40]
Pentane	R601	HC	~20 [33]	A3 [41]
Isohexane		HC	~20 [33]	-
Hexane		HC	~20 [33]	-
Cyclohexane		HC	~20 [33]	A3 [19]
1,1,1,2-tetrafluoroethane	R134a	HFC	1370 [33]	A1 [19]
1,1-difluoroethane	R152a	HFC	133 [33]	A2 [19]
1,1,1,2,3,3,3-heptafluoropropane	R227ea	HFC	3500 [42]	A1 [18]
1,1,1,2,3,3-hexafluoropropane	R236ea	HFC	1410 [33]	-
1,1,1,3,3,3-hexafluoropropane	R236fa	HFC	6300 [42]	A1 [43]
1,1,1,3,3-pentafluoropropane	R245fa	HFC	1050 [33]	B1 [18]
1,1,2,2,3-pentafluoropropane	R245ca	HFC	726 [33]	-
Octafluorocyclobutane	RC318	PFC	10300 [35]	A1 [19]
Methyl-heptafluoropropyl-ether	RE347mcc	HFE	450 [44]	Non-flammable [44]
2,2,2-trifluoroethyl-difluoromethyl-ether	RE245fa2	HFE	659 [45]	-
2,3,3,3-Tetrafluoropropene	R1234yf	HFO	4 [46]	A2L [35]
Trans-1,3,3,3-tetrafluoropropene	R1234ze	HFO	6 [47]	A2L [35]
Trans-1-chloro-3,3,3-trifluoropropene	R1233zd	HFO	7 [48]	A1 [48]

A: Lower toxicity, B: Higher toxicity, 1: Non-flammable, 2: Lower flammability 3: Higher flammability

The selection of the most suitable thermofluid for the proposed solar ORC depends on the decision criteria. For instance, R600a, R600 and cyclohexane show high thermal efficiency and net work output but they have flammability problems. Furthermore, R236fa, R227ea have high GWP, R134a, R152a, R1234yf, R1234ze represents high saturation pressure, and R245fa has toxicity issue. One way to restrain the flammability and GWP of the compounds is blending them with other compounds that have lower flammability and GWP.

In addition to the environmental benefits, the system performance could also be improved by using a mixture as the limitations on the cycle operating conditions and thermodynamic and physical properties are enhanced [49, 50]. Lastly, the selected fluid should not be corrosive to eliminate major corrosion problems in the cycle components in terms of the durability of the system.

5. Conclusion

A small scale solar ORC has been modelled thermodynamically and the cycle simulations with 24 working fluids are studied in this research. In the simulation analyses, the effect of each working fluid on each component as well as the whole cycle at various pressure ratios of the cycle is investigated.

The simulation results reveal that pressure ratio, in other words evaporating pressure of the cycle, has a significant effect on the collector and expander efficiency and therefore, on the net work output and thermal efficiency of the cycle.

The simulation results also showed that, in general, HCs such as trans-2-butene, cis-2-butene, 1-butene, R600a, R600, R601, R601a, neopentane, HFCs such as R227ea, R236fa, and RC318 (PFC) and R1234ze (HFO) yield higher values of net work output of the cycle.

Furthermore, the working fluid plays a key role in the operation of the solar ORC. For instance, fluids with relatively low boiling temperature, such as R134a, R152a, R227ea, R1234yf, and R1234ze, lead to an increase in the evaporation pressure that might limit their application in the collector. The other important parameter is the environmental impacts of the thermo-fluids. For example, although the HCs provide high solar ORC performance, one of the disadvantages of hydrocarbons is their high flammability. In addition to the flammability issue of the fluids, toxicity for R245fa and global warming potential for RC318, R134a and R236fai are the other environmental limitations of these fluids. On the other hand, although, HFEs (RE347mcc and RE245fa2) and HFOs (R1234yf andR1233zd) offer a moderate system performance, they are viable thermo-fluids for the proposed solar ORC based on their thermo-physical characteristics, low GWP and safety issues.

Finally, it is suggested that a mixture of two components can be used in order to eliminate the problems such as flammability, toxicity and global warming potential that might occur when pure components are utilised in the solar ORC.

Acknowledgment

The authors would like to acknowledge financial and in-kind support provided by Future Energy Source (FES) Ltd UK to conduct this research.

References

[1] G. Qiu. Selection of working fluids for micro-CHP systems with ORC. Renewable Energy. 48 (2012) 565-70.
[2] G. Boyle, B. Everett, J. Ramage, T.O. University. Energy systems and sustainability. Oxford University Press Oxford2003.
[3] S. Mekhilef, R. Saidur, A. Safari. A review on solar energy use in industries. Renewable and Sustainable Energy Reviews. 15 (2011) 1777-90.
[4] H. Chen, D.Y. Goswami, E.K. Stefanakos. A review of thermodynamic cycles and working fluids for the conversion of low-grade heat. Renewable and sustainable energy reviews. 14 (2010) 3059-67.
[5] C. He, C. Liu, H. Gao, H. Xie, Y. Li, S. Wu, et al. The optimal evaporation temperature and working fluids for subcritical organic Rankine cycle. Energy. 38 (2012) 136-43.
[6] J. Roy, A. Misra. Parametric optimization and performance analysis of a regenerative Organic Rankine Cycle using R-123 for waste heat recovery. Energy. 39 (2012) 227-35.
[7] D. Manolakos, G. Papadakis, E.S. Mohamed, S. Kyritsis, K. Bouzianas. Design of an autonomous low-temperature solar Rankine cycle system for reverse osmosis desalination. Desalination. 183 (2005) 73-80.
[8] D. Manolakos, G. Papadakis, S. Kyritsis, K. Bouzianas. Experimental evaluation of an autonomous low-temperature solar Rankine cycle system for reverse osmosis desalination. Desalination. 203 (2007) 366-74.
[9] D. Manolakos, G. Kosmadakis, S. Kyritsis, G. Papadakis. On site experimental evaluation of a low-temperature solar organic Rankine cycle system for RO desalination. Solar Energy. 83 (2009) 646-56.
[10] X. Wang, L. Zhao, J. Wang, W. Zhang, X. Zhao, W. Wu. Performance evaluation of a low-temperature solar Rankine cycle system utilizing R245fa. Solar Energy. 84 (2010) 353-64.
[11] J. Wang, L. Zhao, X. Wang. An experimental study on the recuperative low temperature solar Rankine cycle using R245fa. Applied Energy. 94 (2012) 34-40.
[12] H. Yamaguchi, X. Zhang, K. Fujima, M. Enomoto, N. Sawada. Solar energy powered Rankine cycle using supercritical CO 2. Applied Thermal Engineering. 26 (2006) 2345-54.
[13] X.-R. Zhang, H. Yamaguchi, D. Uneno. Experimental study on the performance of solar Rankine system using supercritical CO2. Renewable Energy. 32 (2007) 2617-28.
[14] R. Rayegan, Y. Tao. A procedure to select working fluids for Solar Organic Rankine Cycles (ORCs). Renewable Energy. 36 (2011) 659-70.
[15] A.M. Delgado-Torres, L. García-Rodríguez. Analysis and optimization of the low-temperature solar organic Rankine cycle (ORC). Energy Conversion and Management. 51 (2010) 2846-56.
[16] M. Marion, I. Voicu, A.-L. Tiffonnet. Study and optimization of a solar subcritical organic Rankine cycle. Renewable Energy. 48 (2012) 100-9.
[17] M. Wang, J. Wang, Y. Zhao, P. Zhao, Y. Dai. Thermodynamic analysis and optimization of a solar-driven regenerative organic Rankine cycle (ORC) based on flat-plate solar collectors. Applied Thermal Engineering. 50 (2013) 816-25.

[18] S. Baral, K.C. Kim. Thermodynamic modeling of the solar organic Rankine cycle with selected organic working fluids for cogeneration. Distributed Generation & Alternative Energy Journal. 29 (2014) 7-34.
[19] B.F. Tchanche, G. Papadakis, G. Lambrinos, A. Frangoudakis. Fluid selection for a low-temperature solar organic Rankine cycle. Applied Thermal Engineering. 29 (2009) 2468-76.
[20] H. Helvaci, Z.A. Khan. Mathematical modelling and simulation of multiphase flow in a flat plate solar energy collector. Energy Conversion and Management. 106 (2015) 139-50.
[21] S. Klein. Calculation of flat-plate collector loss coefficients. Solar Energy. 17 (1975) 79-80.
[22] F.P. Incropera. Fundamentals of heat and mass transfer. John Wiley & Sons2011.
[23] M. Shah. Chart correlation for saturated boiling heat transfer: equations and further study. (1982).
[24] H.U. Helvaci, Z.A. Khan. Experimental study of thermodynamic assessment of a small scale solar thermal system. Energy Conversion and Management. 117 (2016) 567-76.
[25] P. Kolasiński. The Influence of the Heat Source Temperature on the Multivane Expander Output Power in an Organic Rankine Cycle (ORC) System. Energies. 8 (2015) 3351-69.
[26] S. Quoilin. Sustainable Energy Conversion Through the Use of Organic Rankine Cycles for Waste Heat Recovery and Solar Applications. University of Liège (Belgium2011.
[27] Z. Gnutek, P. Kolasiński. The application of rotary vane expanders in organic rankine cycle systems—thermodynamic description and experimental results. Journal of Engineering for Gas Turbines and Power. 135 (2013) 061901.
[28] S. Quoilin, S. Declaye, B.F. Tchanche, V. Lemort. Thermo-economic optimization of waste heat recovery Organic Rankine Cycles. Applied thermal engineering. 31 (2011) 2885-93.
[29] Y.M. Kim, D.G. Shin, C.G. Kim. Optimization of design pressure ratio of positive displacement expander for vehicle engine waste heat recovery. Energies. 7 (2014) 6105-17.
[30] J. Wang, Z. Yan, M. Wang, S. Ma, Y. Dai. Thermodynamic analysis and optimization of an (organic Rankine cycle) ORC using low grade heat source. Energy. 49 (2013) 356-65.
[31] Q. Liu, A. Shen, Y. Duan. Parametric optimization and performance analyses of geothermal organic Rankine cycles using R600a/R601a mixtures as working fluids. Applied Energy. 148 (2015) 410-20.
[32] E. Lemmon, M. Huber, M. McLinden. NIST reference database 23: reference fluid thermodynamic and transport properties-REFPROP, version 9.1. Standard Reference Data Program. (2013).
[33] H. Zhai, L. Shi, Q. An. Influence of working fluid properties on system performance and screen evaluation indicators for geothermal ORC (organic Rankine cycle) system. Energy. 74 (2014) 2-11.
[34] J. Bao, L. Zhao. A review of working fluid and expander selections for organic Rankine cycle. Renewable and Sustainable Energy Reviews. 24 (2013) 325-42.
[35] J. Vivian, G. Manente, A. Lazzaretto. A general framework to select working fluid and configuration of ORCs for low-to-medium temperature heat sources. Applied Energy. 156 (2015) 727-46.
[36] W. Husband, A. Beyene. Low-grade heat-driven Rankine cycle, a feasibility study. International Journal of Energy Research. 32 (2008) 1373-82.
[37] H. Helvaci, Z.A. Khan. Heat transfer and entropy generation analysis of HFE 7000 based nanorefrigerants. International Journal of Heat and Mass Transfer. 104 (2017) 318-27.
[38] E. Granryd. Hydrocarbons as refrigerants—an overview. International journal of refrigeration. 24 (2001) 15-24.

[39] C.M. Invernizzi, P. Iora, M. Preßinger, G. Manzolini. HFOs as substitute for R-134a as working fluids in ORC power plants: A thermodynamic assessment and thermal stability analysis. Applied Thermal Engineering. 103 (2016) 790-7.
[40] N. Designation. Safety Classification of Refrigerants. ASHRAE Standard, ANSI/ASHRAE. (1993).
[41] J.R. Juhasz, L.D. Simoni. A review of potential working fluids for low temperature organic rankine cycles in waste heat recovery. 3rd International Seminar on ORC, Brussels, Belgium2015. pp. 12-4.
[42] Z. Wang, N. Zhou, J. Guo, X. Wang. Fluid selection and parametric optimization of organic Rankine cycle using low temperature waste heat. Energy. 40 (2012) 107-15.
[43] G. Kosmadakis, D. Manolakos, S. Kyritsis, G. Papadakis. Comparative thermodynamic study of refrigerants to select the best for use in the high-temperature stage of a two-stage organic Rankine cycle for RO desalination. Desalination. 243 (2009) 74-94.
[44] W.-T. Tsai. Environmental risk assessment of hydrofluoroethers (HFEs). Journal of hazardous materials. 119 (2005) 69-78.
[45] B. Striebig, A.A. Ogundipe, M. Papadakis. Engineering applications in sustainable design and development. Nelson Education2015.
[46] F. Ayachi, E.B. Ksayer, A. Zoughaib, P. Neveu. ORC optimization for medium grade heat recovery. Energy. 68 (2014) 47-56.
[47] M. Feidt, A. Kheiri, S. Pelloux-Prayer. Performance optimization of low-temperature power generation by supercritical ORCs (organic Rankine cycles) using low GWP (global warming potential) working fluids. Energy. 67 (2014) 513-26.
[48] F. Molés, J. Navarro-Esbrí, B. Peris, A. Mota-Babiloni, Á. Barragán-Cervera, K.K. Kontomaris. Low GWP alternatives to HFC-245fa in Organic Rankine Cycles for low temperature heat recovery: HCFO-1233zd-E and HFO-1336mzz-Z. Applied Thermal Engineering. 71 (2014) 204-12.
[49] J. Wang, L. Zhao, X. Wang. A comparative study of pure and zeotropic mixtures in low-temperature solar Rankine cycle. Applied Energy. 87 (2010) 3366-73.
[50] J. Song, C.-w. Gu. Analysis of ORC (Organic Rankine Cycle) systems with pure hydrocarbons and mixtures of hydrocarbon and retardant for engine waste heat recovery. Applied Thermal Engineering. 89 (2015) 693-702.